

Supporting Information

Cytoskeleton-inspired Hydrogel Ionotronics for Tactile Perception and Electroluminescent Display in Complex Mechanical Environments†

Chenchen Dai,^{‡ab} Yang Wang,^{‡a} Yicheng Shan,^{‡a} Chao Ye,^{ca} Zhuochen Lv,^a Shuo Yang,^a Leitao

Cao,^{da} Jing Ren,^{*a} Haipeng Yu,^b Shouxin Liu,^b Zhengzhong Shao,^e Jian Li,^b Wenshuai Chen^{*b} and

Shengjie Ling^{*af}

^aSchool of Physical Science and Technology, ShanghaiTech University, 393 Middle Huaxia Road,
Shanghai 201210, China.

^bKey Laboratory of Bio-based Material Science and Technology, Ministry of Education, Northeast
Forestry University, Harbin 150040, China.

^cSchool of Textile & Clothing, Yancheng Institute of Technology, Jiangsu 224051, China.

^dInstitute of Zhejiang University-Quzhou, 78 Jiuhua Boulevard North, Quzhou 324000, China.

^eState Key Laboratory of Molecular Engineering of Polymers, Department of Macromolecular Science,
Laboratory of Advanced Materials, Fudan University, Shanghai 200433, China.

^fShanghai Clinical Research and Trial Center, Shanghai 201210, People's Republic of China.

*Corresponding author

E-mail: renjing@shanghaitech.edu.cn (Jing Ren), chenwenshuai@nefu.edu.cn (Wenshuai Chen),

lingshj@shanghaitech.edu.cn (Shengjie Ling)

Supplementary Note 1. Methods

Calculation of l and ξ . The elasto-adhesive length l was calculated according to Eq. (1) in the main text. The fracture energy Γ was calculated through a set of tensile tests, i.e., tensile tests on two samples; one without a notch and one with a notch (Fig. S3, ESI†):

$$\Gamma = H \int_1^{\lambda_C} s d\lambda \quad (S1)$$

where H is the effective length of the unnotched sample at the beginning of the tensile test, λ_C is the strain at which the crack of the notched sample begins to propagate, and s is the nominal stress. In Eq. (1), E is the Young's modulus, which was determined based on the first portion of the stress-strain curve, i.e., the equilibrium region, which might be located at the post-yielding region when the yield stress and strain are adequately small. The value of E is of high significance when calculating the l ; thus, it is vital to measure the Young's modulus at the near-linear region far ahead of the catastrophic failure point.

The crack-tip load-transfer length ξ represents the length scale of the failure zone around the crack tip (Fig. S4, ESI†). The ξ was calculated according to Eq. (2) in the main text. Hence, in addition to Γ , the critical energy per unit volume for material failure W_* was also calculated as follows:

$$W_* = \frac{\text{Area enclosed by the force - displacement curve}}{\text{Volume of sample}} \quad (S2)$$

Fatigue threshold calculation. A set of cyclic tensile tests was performed using a pre-notched and an unnotched sample. The strain energy density and the energy release rate

were calculated according to Eqs. (3-4) in the main text. In these equations, N is the number of cycles of tensile loading, λ_A is the maximum elongation (i.e., strain limit), and $c(N)$ is the crack length at the N^{th} cycle. To determine the $c(N)$ for each N , pixel judgment based on the polarized video recorded during the cyclic tensile tests was performed. The value of $c(N)$ was determined based on the initial frames when unloading relaxation occurred. In order to obtain the fatigue threshold Γ_0 , dc/dN and G were plotted first to find the inflection point, and then, linear fitting was performed on the data points whose G was larger than the inflection point, and the intersection point with the X-axis was the Γ_0 .

Orientation distribution B_Ψ calculation. The small angle X-ray scattering orientation distribution factor B_{obs} was calculated by:

$$B_{obs} = \frac{\int I(s, \varphi) d\varphi}{I_{max, s}} \quad (S3)$$

where s is the reciprocal space vector, φ is the azimuthal angle of the pattern. It is restricted in the azimuthal region of -45 to 45 degrees. $I_{max, s}$ is the value of the maximum intensity at a certain s . The $I(s, \varphi)$ was plotted through the divided data processing of the whole pattern. The s was determined by:

$$s = q/2\pi \quad (S4)$$

where q is the diffraction vector. For each $I(s, \varphi)$ plot, a corresponding certain $I(q)$ plot could be extracted. All plots were constructed using the Fit2D software. Subsequently, q

was set to be the maximum abscissa value in the $I(q)$ plot. Thereafter, sets of B_{obs} and s values could be obtained, correlating each B_{obs} to one certain s . Furthermore, the linear fit over $sB_{obs} - s$ was conducted by:

$$sB_{obs}(s) = sB_{\Psi} + \frac{1}{L} \quad (S5)$$

where B_{Ψ} reflects the orientation distribution and L represents the mean length of the scatterers. Accordingly, the slope of the linear fit over $sB_{obs} - s$ was the approximated and quantized value of B_{Ψ} , where the smaller the B_{Ψ} , the higher the orientation degree along the direction of interest.

Fatigue threshold calculation

The fatigue fracture behavior of CIHI also evaluated through cyclic tensile loading-unloading tests,¹ which were performed with unnotched and single-edge pre-notched samples. During cyclic loading, a triangular loading profile was applied (Fig. S5, ESI†). The maximum stretch was kept constant at λ_{max} , while the minimum stretch was kept at 1. The nominal stress-stretch curves of the unnotched samples were obtained over N cycles of applied stretch λ^A . The strain energy density W of the unnotched sample at the N_{th} cycle of applied stretch λ^A can be calculated as:

$$W(\lambda^A, N) = \int_1^{\lambda^A} s d\lambda \quad (3)$$

where s and λ denote the measured nominal stress and stretch, respectively. Accordingly, the same cyclic stretch λ was applied to the pre-notched sample, measuring the evolution

of the cut length in the undeformed state c with the number of cycles N . The applied energy release rate G in the pre-notched sample at the N^{th} cycle of applied stretch λ^A can be calculated as:²

$$G(\lambda^A, N) = 2K(\lambda^A) \times c(N) \times W(\lambda^A, N) \quad (4)$$

where K is a slow-varying function of the applied stretch expressed as $3/\sqrt{\lambda^A}$, c is the current crack length in the undeformed configuration, and W is the strain energy density measured in the unnotched sample. The critical energy release rate G_c , which is equal to the fatigue threshold G_0 , can be approximately obtained by linearly extrapolating the dc/dN vs. G curve to intercept with the abscissa. When $G < G_c$, the fatigue crack will not propagate under infinite cycles of loads.

Supplementary Note 2. The acquisition of 180 data points

First, the microcontroller continuously collects the voltage signal generated by the TENG at a sampling rate of 100 Hz. When the TENG is touched, a pair of positive and negative signal peaks will be generated; when the TENG is not touched, the voltage signal is 0. These voltage signal values are continuously transmitted to the software side by the microcontroller, and are buffered in a list of a certain length. When the touch occurs, the software recognizes that the voltage signal suddenly changes from 0, and the algorithm will automatically flash back and intercept the 49 data points before the signal value and record the 130 data points after the signal value. After 180 data points are acquired, the data points are automatically fed to the machine learning model to deduce the type of material touched on the TENG.

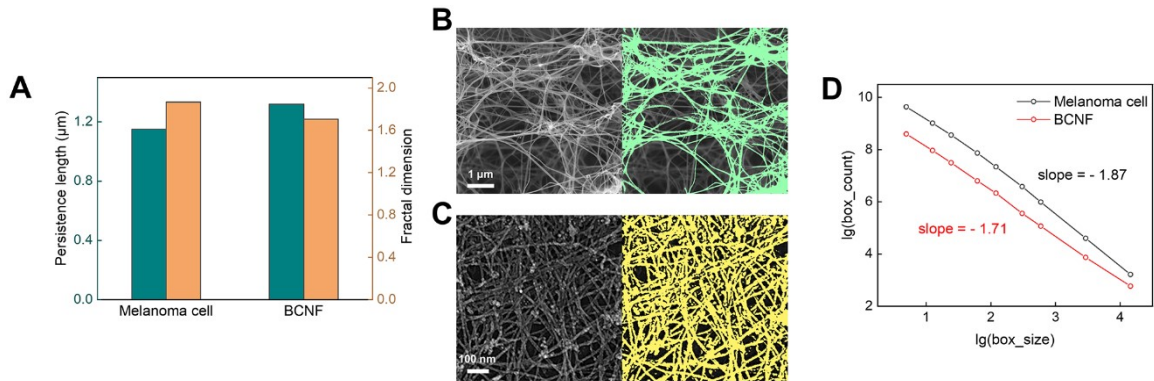


Fig. S1 (A) Comparison of the fractal dimension and persistence length of the filamentous networks in Melanoma cell and BCNF. (B) SEM image of BCNF network. (C) SEM image of the cytoskeleton of a B16F1 mouse melanoma cell. This image has been adopted from Ref.³ with permission. Copyright 2009, Springer Nature. (D) Double logarithm plot of fractal dimension calculation. The fractal dimension was equal to the negative value of slope.

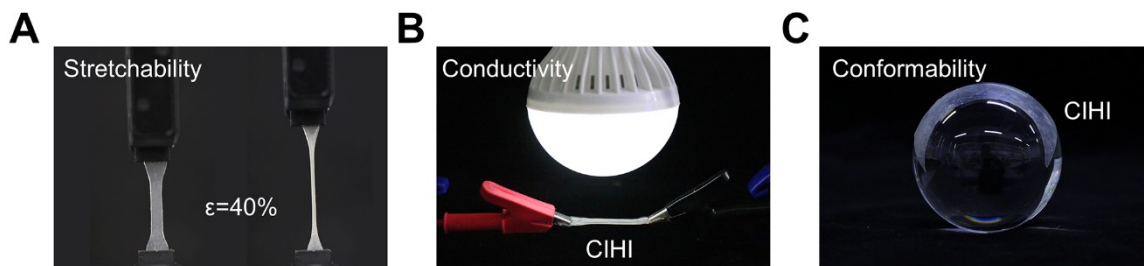


Fig. S2 (A) CIHI can be elongated to 40% without fracture. (B) CIHI is conductive. (C) CIHI can be self-adapted to spherical surfaces.

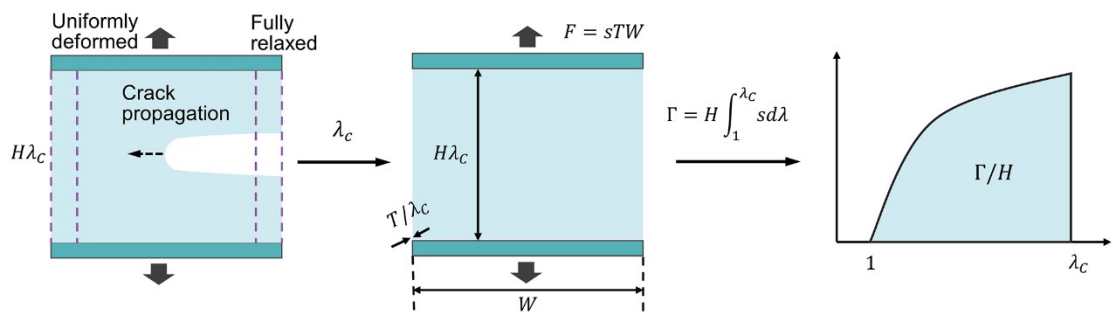


Fig. S3 Schematic illustration of the method used to calculate the fracture energy. This schematic were adopted from Ref.⁴ with permission. Copyright 2014, The Royal Society of Chemistry.

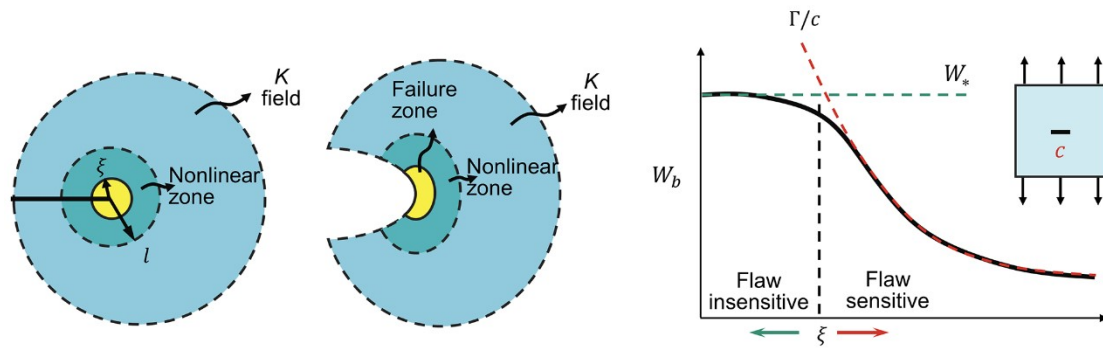


Fig. S4 Schematic depicting the length scale of l and ξ around the crack tip. This schematic was adopted from Ref.⁵ with permission. Copyright 2021, Annual Reviews.

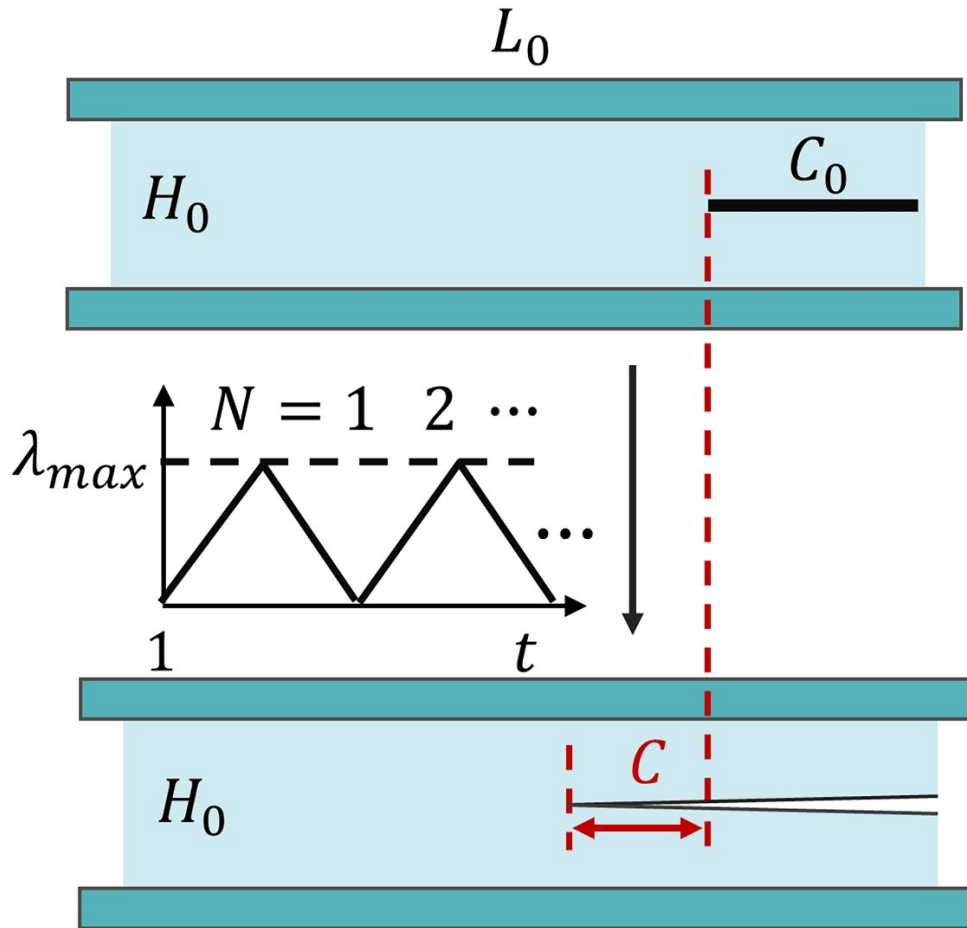


Fig. S5 Schematics of the method used to calculate the fatigue threshold. The length of the crack was measured from the polarized images of the pre-notched sample during the cyclic stretching tests. This schematic was adopted from Ref.² with permission. Copyright 2021, CC BY-NC 4.0.

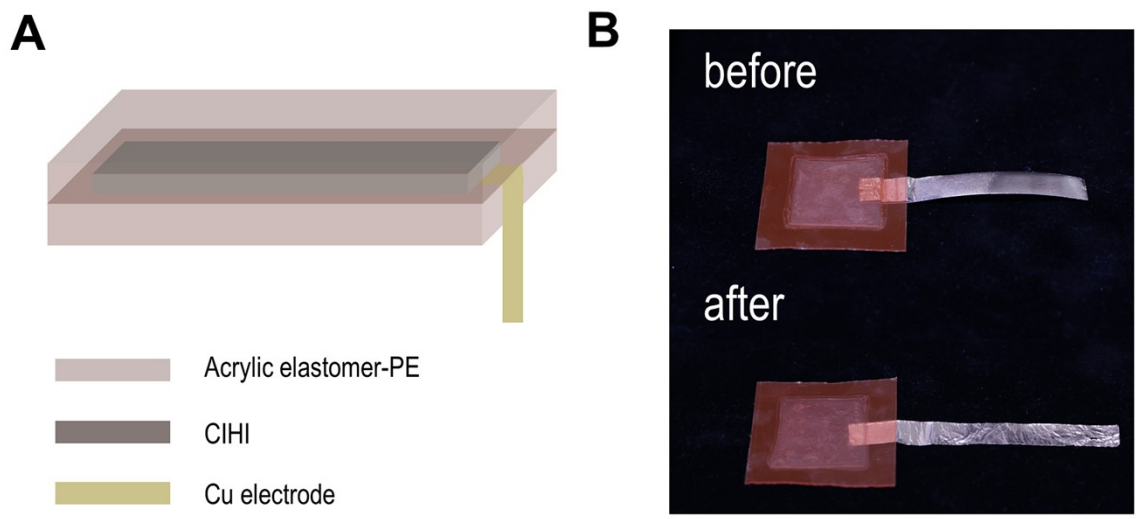


Fig. S6 (A) Schematic illustration of the assembled CIHI-TENG. (B) Photograph showing the structural integrity of CIHI-TENG maintained during 100,000 flapping-type contact separation tests.

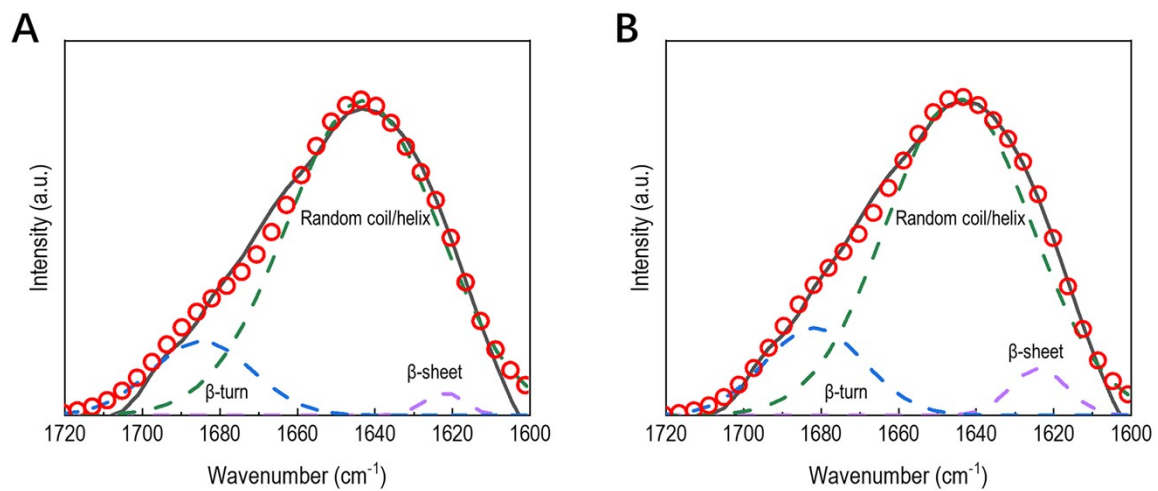


Fig. S7 Results of deconvolution of amide I peak in FTIR spectrum before (A) and after (B) 100,000 contact separations of CIHI-TENG.

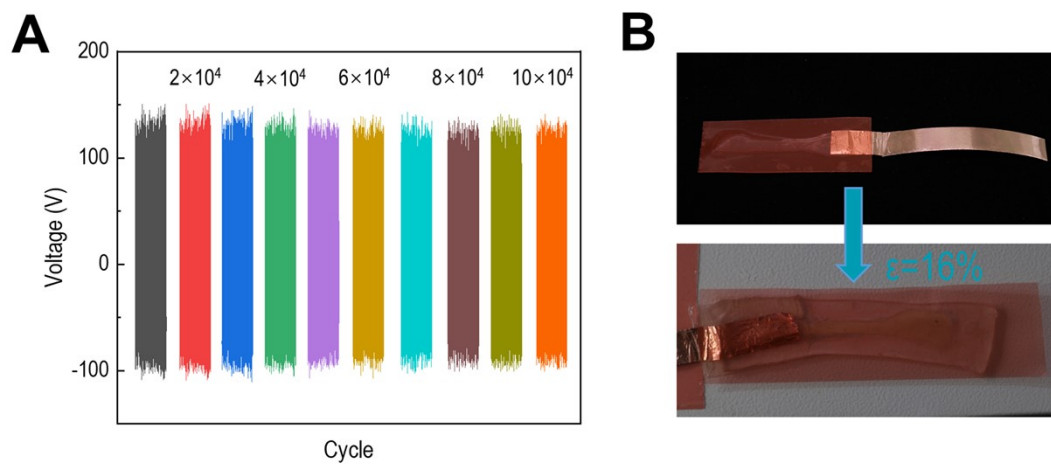


Fig. S8 (A) Triboelectric stability of extremely deformed CIHI-TENG for 100,000 cycles of contact-separation processing. (B) Photograph showing the structural integrity of deformed CIHI-TENG maintained during 100,000 flapping-type contact separation tests.

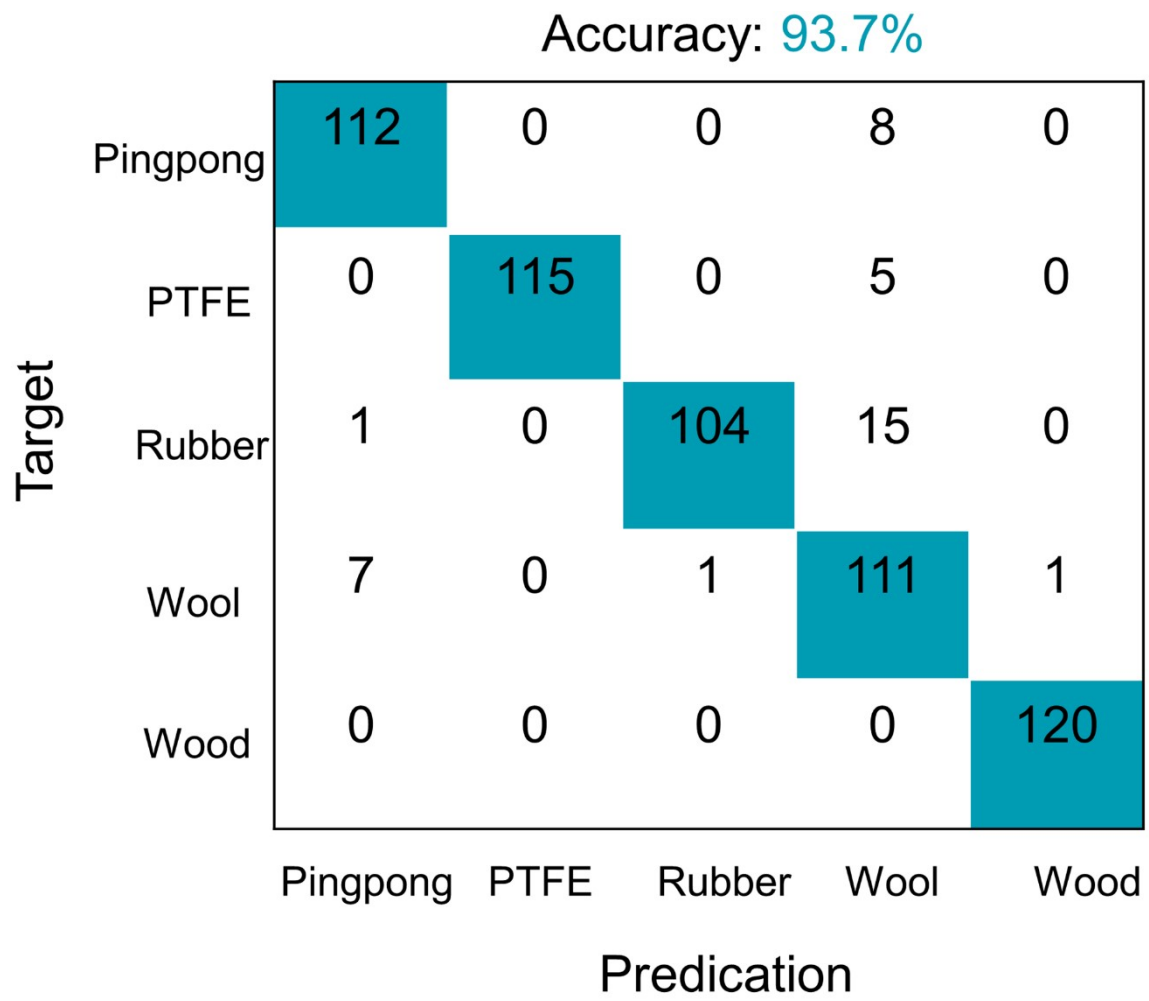


Fig. S9 The sorting success accuracy of different types of balls in 120 predictions.

A Accuracy: 87.7%

Target	Ceramics	200	0	0
	Glass	21	179	0
	DVD	44	9	147
		Ceramics	Glass	DVD
		Predication		

B

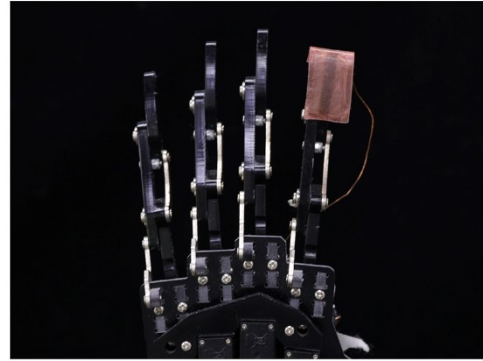


Fig. S10 (A) The sorting success accuracy of different types of sharp objects in 200 predictions. (B) CIHI-TENG remained intact after identifying sharp objects.

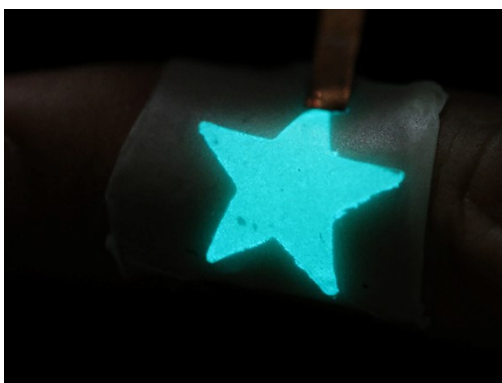


Fig. S11 Photograph showing the attachment of CIHI-ES to human finger.

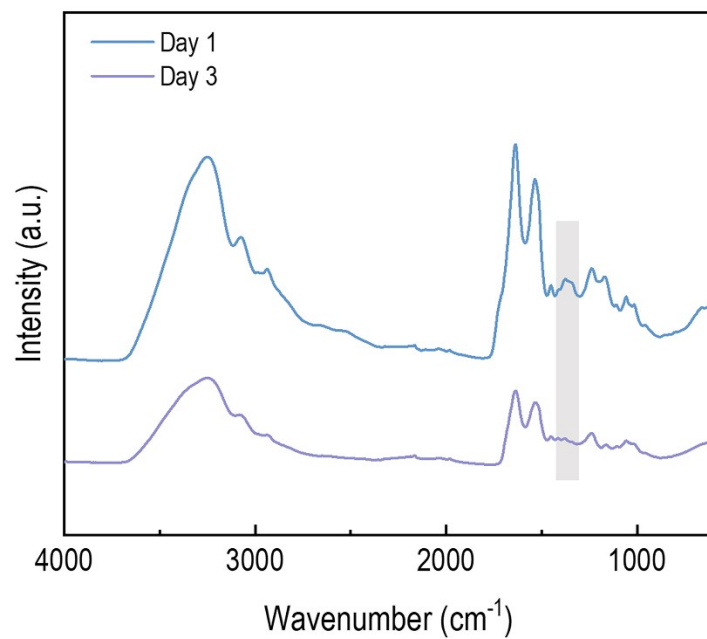


Fig. S12 FTIR spectra of CIHI on day 1 (blue) and day 3 (purple). The characteristic absorption band of the FA (1381 cm⁻¹) disappeared in the spectrum for day 3, demonstrating the removal of FA.

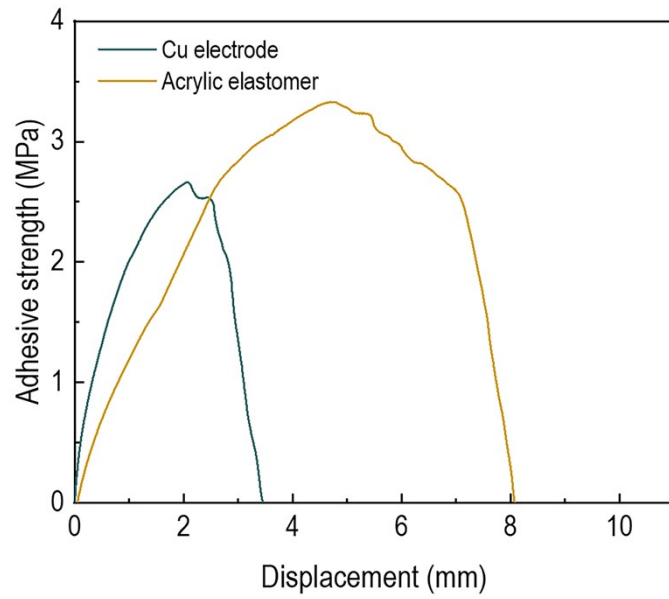


Fig. S13 Adhesion strength–displacement curves obtained from the lap-shear test for CIHI on Cu electrode and Acrylic elastomer substrates.

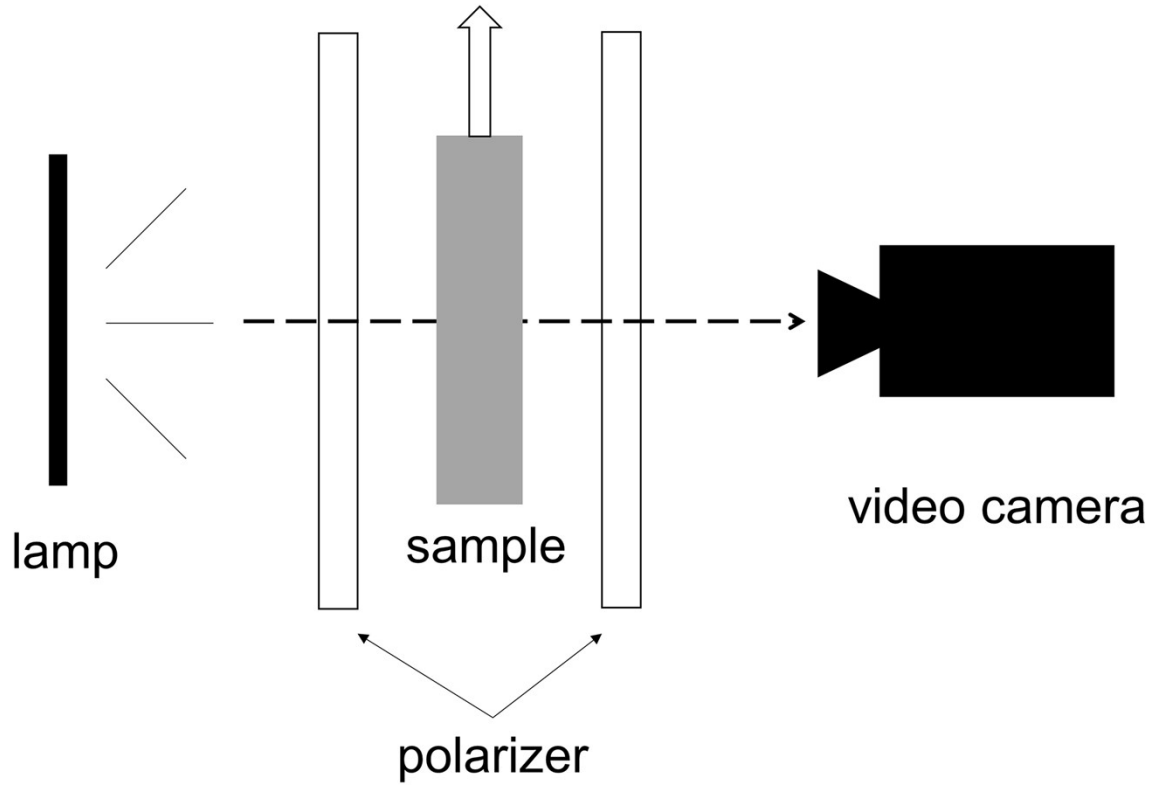


Fig. S14 Schematic diagram of the polarizing optical system in tensile test.

Table S1. The mechanical properties of CIHI, MTCIHI, Hydrated BCNF aerogel, SFI, VHB and EL layer.

Sample	Strength (MPa)	Strain of failure (%)	Young's modulus (MPa)	Toughness (MJ m ⁻³)	Yield strength (MPa)
CIHI (AC)	4.8±0.6	63±10	10±4	1.8±0.5	-
CIHI (MT)	7±2	37±11	74±33	1.8±0.8	4±1
Hydrated BNC aerogel	1.4±0.2	27±4	2.7±0.5	0.16±0.04	-
SFI	0.27±0.04	362±70	0.7±0.2	0.7±0.2	0.12±0.02
VHB	0.93±0.04	1884±92	0.35±0.01	9.3±0.5	-
EL layer	0.4±0.1	505±97	0.12±0.01	2±1	-

Reference

1. S. Lin, X. Liu, J. Liu, H. Yuk, H.-C. Loh, G. A. Parada, C. Settens, J. Song, A. Masic and G. H. McKinley, *Sci. Adv.*, 2019, **5**, eaau8528.
2. X. Li, K. Cui, T. Kurokawa, Y. N. Ye, T. L. Sun, C. Yu, C. Creton and J. P. Gong, *Sci. Adv.*, 2021, **7**, eabe8210.
3. R. H. Gavin, *Cytoskeleton methods and protocols*, Springer, 2009.
4. X. Zhao, *Soft Matter*, 2014, **10**, 672-687.
5. R. Long, C.-Y. Hui, J. P. Gong and E. Bouchbinder, *arXiv preprint arXiv:2004.03159*, 2020.